

Open Charm Production at STAR

Haibin Zhang[†] (for the STAR Collaboration) [§]

[†] Physics Department, Brookhaven National Laboratory, Upton, NY, 11953, USA
E-mail: haibin@bnl.gov

Abstract. We present the open charm spectra at mid-rapidity from direct reconstruction of D^0 , D^* and D^\pm in d+Au collisions at $\sqrt{s_{NN}}=200$ GeV using the STAR detector at RHIC. The indirect electron/positron measurements via charm semileptonic decays in p+p and d+Au collisions are also reported. The total $c\bar{c}$ cross section per nucleon-nucleon collision is extracted from both direct and indirect measurements and are consistent with each other. By combining the D^0 and semileptonic measurements together, the cross section of $1.4\pm 0.2\pm 0.4$ mb is higher than expectations from PYTHIA and other pQCD calculations. The open charm p_T distribution from direct measurements covers the p_T range up to ~ 10 GeV/c and follows a power-law distribution.

PACS numbers: 25.75.-q, 25.75.Dw, 13.25.Ft

Submitted to: *J. Phys. G: Nucl. Phys.*

1. Introduction

Due to the relatively large mass of the heavy quarks which requires large energies for their creation, the study of heavy flavor productions provides a unique tool to test the perturbative Quantum Chromodynamics (pQCD) calculations for heavy quark predictions [1]. The energy dependence of the total $c\bar{c}$ cross section measured from experiments is an important variable to constrain various parameters in the pQCD calculations [2]. It is predicted that the charm quarks are mostly produced from the initial fusion of gluons in a high energy hadron-hadron collision [3]. Thus, the measurement of open charm hadron production is an important tool to study the initial parton distribution function in the colliding nucleons. In relativistic heavy ion collisions, the open charm p_T spectrum may be modified due to parton energy loss in the deconfined hot and dense medium. However, this energy loss is predicted to be significantly smaller compared to light quark hadrons due to the “deadcone effect” [4]. As a consequence, an increased D/π ratio as a function of p_T is expected in central A+A collisions compared to p+p collisions at the same beam energy. Therefore, the measurement of the open charm p_T spectrum can provide insights into the properties of the matter formed in the

[§] For the full author list and acknowledgements, see Appendix “Collaboration” in this volume.

relativistic heavy ion collisions. Furthermore, the production of open charm hadrons in the same collision system provides a comparison baseline to test the J/ψ production mechanism in the relativistic heavy ion collisions at RHIC energies since some theories predict a J/ψ enhancement due to the charm quark coalescence effect [5, 6, 7, 8, 9] while others predict a J/ψ suppression due to the color screening effect [10].

2. Measurements

The data used for the direct D^0 , D^* and D^\pm reconstruction and the charm semileptonic decay analysis were taken during the 2003 RHIC run in d+Au and p+p collisions at $\sqrt{s_{NN}}=200$ GeV in the STAR experiment. A minimum bias d+Au collision trigger was defined by requiring at least one spectator neutron in the Au beam outgoing direction depositing energy in the Zero Degree Calorimeter (ZDC). A total of 15 million minimum bias triggered d+Au collision events were used in the D^0 , D^* and D^\pm analysis. The data samples used in the electron analysis in d+Au and p+p collisions were described in Ref. [11].

2.1. Direct D Meson Reconstruction

The primary tracking device of the STAR detector is the Time Projection Chamber (TPC) which measures the kinematics of charged particles. Via the energy loss (dE/dx) in the TPC, charged kaons and pions can be identified with their momenta up to ~ 0.75 GeV/c. Due to the relatively small decay lengths ($c\tau \sim 100\mu\text{m}$) of the D^0 , D^* and D^\pm , the limited TPC track projection resolution does not allow the decay topology identification by displaced vertices for open charm mesons from the primary collision vertex. Thus the event-mixing technique was used to reconstruct the invariant mass spectra of the D mesons. Detailed explanation of this method was addressed in Ref. [12, 13, 14].

The low p_T ($p_T < 3$ GeV/c) D^0 meson was reconstructed through the decay of $D^0 \rightarrow K^-\pi^+$ ($\bar{D}^0 \rightarrow K^+\pi^-$) which has a branching ratio of 3.83%. The oppositely charged $K\pi$ invariant mass distribution after the combinatorial background subtraction from event-mixing and a linear residual background subtraction is shown in Panel (a) of Fig. 1 with a clear D^0 signal visible. This distribution was fit with a Gaussian function and the mass and width of the D^0 was found to be 1863 ± 3 MeV/ c^2 (1864.5 ± 0.5 MeV/ c^2 in the Particle Data Group [15]) and 13.8 ± 2.8 MeV/ c^2 , respectively.

The $D^{*\pm}$ mesons were reconstructed through the decay of $D^{*+} \rightarrow D^0\pi_s^+$ ($D^{*-} \rightarrow \bar{D}^0\pi_s^-$) with a branching ratio of 68%. Specific treatment for the soft pion daughter π_s^\pm was performed which required its p_T and p between 0.1 to 1 GeV/c and the ratio of the D^0 to π_s momentum $p(D^0)/p(\pi_s) > 9$ since the π_s has an average momentum of about 50 MeV/c. The invariant mass of the kaon and pion candidates $M(K\pi)$ was calculated and required to satisfy the D^0 mass $1.82 < M(K\pi) < 1.9$ GeV/ c^2 . Then a soft pion candidate with its charge opposite to that of the kaon candidate was combined with the

D^0 candidate to calculate the invariant mass of a D^* candidate $M(K\pi\pi_s)$. Panel (b) of Fig. 1 shows the distribution of the invariant mass difference $\Delta M = M(K\pi\pi_s) - M(K\pi)$ after background subtractions. A clear signal is seen around the nominal value of $M(D^*) - M(D^0)$. This distribution was fit with a Gaussian function and the mass difference and the width was found to be $146.37 \pm 0.15 \text{ MeV}/c^2$ ($145.42 \pm 0.05 \text{ MeV}/c^2$ in the PDG) and $0.57 \pm 0.16 \text{ MeV}/c^2$, respectively.

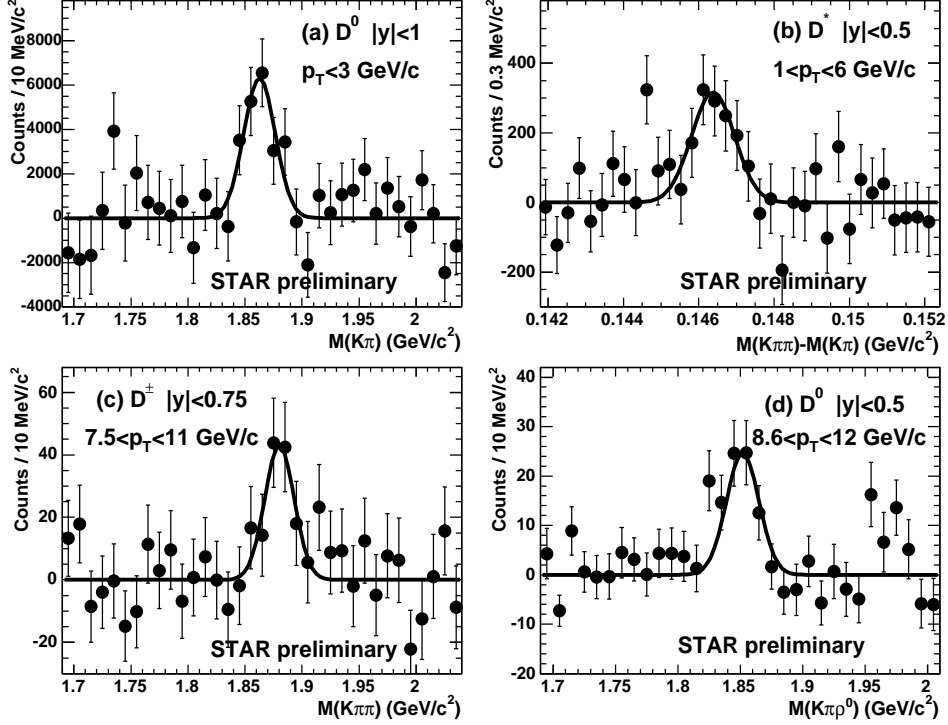


Figure 1. The invariant mass distribution after the mixed-event background subtraction and a further linear background subtraction of $M(K\pi)$ for the low p_T ($p_T < 3 \text{ GeV}/c$) $D^0 + \bar{D}^0$ in Panel (a), $\Delta M = M(K\pi\pi_s) - M(K\pi)$ for the D^{\pm} in Panel (b), $M(K\pi\pi)$ for the D^{\pm} in Panel (c), $M(K\pi\rho^0)$ for the high p_T ($8.6 < p_T < 12 \text{ GeV}/c$) $D^0 + \bar{D}^0$ in Panel (d), respectively.

The D^{\pm} signal was reconstructed through the decay of $D^+ \rightarrow K^-\pi^+\pi^+$ ($D^- \rightarrow K^+\pi^-\pi^-$) with a branching ratio of 9.1%. The invariant mass distribution of $M(K\pi\pi)$ after background subtractions is shown in Panel (c) of Fig. 1 with the D^{\pm} rapidity $|y| < 0.75$ and $7.5 < p_T < 11 \text{ GeV}/c$. A Gaussian function was fit to this distribution and the mass and width was found to be $1880 \pm 5 \text{ MeV}/c^2$ ($1869.3 \pm 0.5 \text{ MeV}/c^2$ in the PDG) and $16.2 \pm 8 \text{ MeV}/c^2$, respectively.

The high p_T ($8.6 < p_T < 12 \text{ GeV}/c$) D^0 was independently reconstructed through the decay of $D^0 \rightarrow K^-\pi^+\rho^0$ ($\bar{D}^0 \rightarrow K^+\pi^-\rho^0$) which has a branching ratio 6.2%. The analysis was similar to that for the low p_T D^0 except that an additional $\pi^+\pi^-$ pair with its invariant mass $0.62 < M(\pi^+\pi^-) < 0.86$ was combined with the selected kaon and pion candidates for a D^0 candidate. The invariant mass distribution for $M(K\pi\rho^0)$ ($=M(K\pi\pi\pi)$) after background subtractions is shown in Panel (d) of Fig. 1. This

distribution was fit with a Gaussian function and the mass and the width was found to be 1850 ± 5 MeV/c² and 13.6 ± 4 MeV/c², respectively.

2.2. Single Electron Analysis

A prototype time-of-flight system (TOFr) [16, 17] based on the multi-gap resistive plate chamber technology was installed in STAR with an azimuthal angle coverage $\Delta\phi \simeq \pi/30$ and pseudorapidity range $-1 < \eta < 0$. Besides its capability of hadron identification, electrons/positrons could be identified at $p_T < 3$ GeV/c by the combination of velocity (β) from TOFr and dE/dx from TPC measurements. In addition, electrons can also be identified with $2 < p_T < 4$ GeV/c in TPC since hadrons have lower dE/dx due to the relativistic rise of the dE/dx of electrons. The inclusive spectra for the low p_T electrons/positrons measured from TOFr+TPC are shown in Fig. 2 as solid symbols and the spectra for higher p_T electrons from TPC only are shown as open circles for p+p (left) and d+Au (right), respectively.

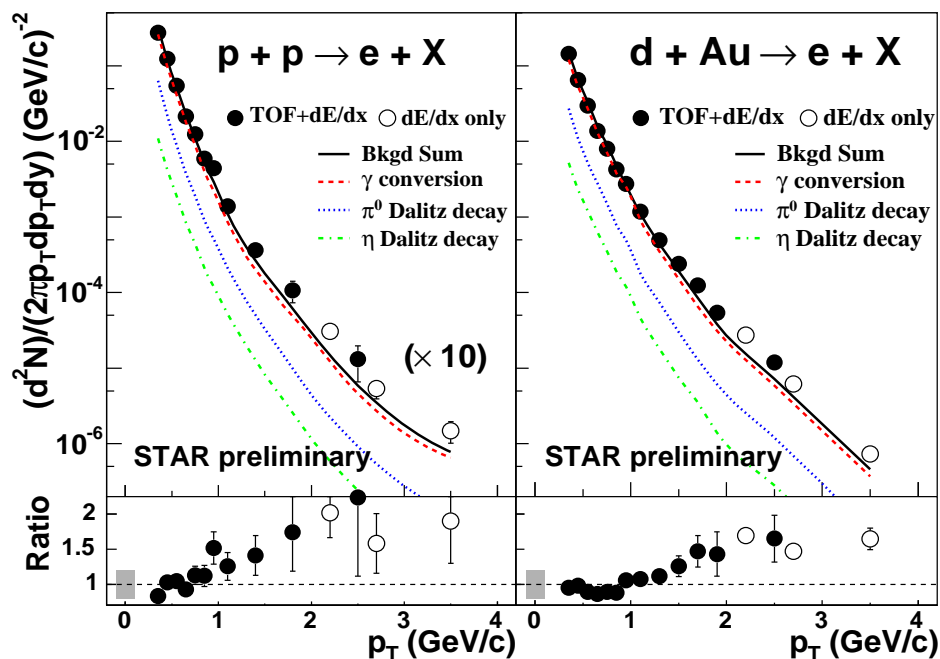


Figure 2. Upper panels: Electron distributions from p+p (left) and d+Au (right) collisions. Bottom panels: Ratios of inclusive electrons over the total backgrounds. The gray bands represent the systematic uncertainties.

The dominant sources of the electron background are the photon conversions $\gamma \rightarrow e^+e^-$ (dashed curves in Fig. 2) and $\pi^0 \rightarrow \gamma e^+e^-$ Dalitz decay (dotted curves) and η Dalitz decay (dash-dotted curves). To measure these photonic electron background spectra, the invariant mass of the e^+e^- pairs were constructed from an electron (positron) in TOFr and every positron (electron) candidate in TPC. The sum of these photonic background is shown as the solid curves in Fig. 2. In the bottom panel of

Fig. 2, the ratio of the inclusive electron/positron spectra and the background is shown and clear signal excesses are visible with $p_T > 1$ GeV/c.

3. Results

3.1. Total $c\bar{c}$ Cross Section

From the direct low p_T D^0 reconstruction in the d+Au collisions, the invariant yield $d^2N/2\pi p_T dp_T dy$ as a function of p_T after efficiency and acceptance correction was extracted in four p_T bins at $p_T < 3$ GeV/c. Using an exponential fit to the invariant yield in transverse mass (m_T), the midrapidity yield dN/dy for D^0 was found to be $0.028 \pm 0.004(stat.) \pm 0.008(sys.)$. We also performed a fit with the combined results of D^0 and electron distributions in d+Au collisions, assuming that the D^0 spectrum follows a power law in p_T and that the remaining electrons after the background subtractions are charm semileptonic decays. The yield difference between the above two fitting methods is much smaller than the statistical uncertainties.

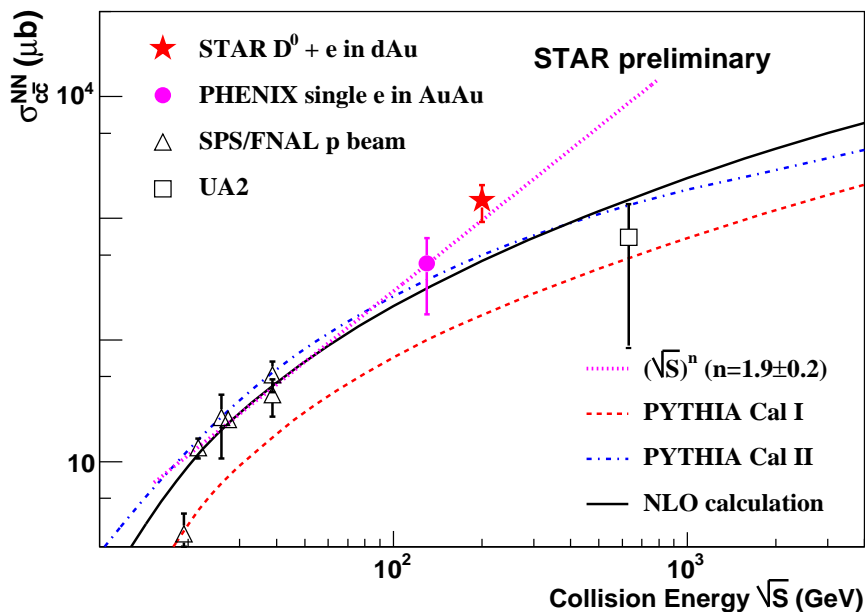


Figure 3. The total $c\bar{c}$ cross section per nucleon-nucleon collision vs. the collision energy. The dotted line is a power-law fit. The dashed and dash-dotted curves are PYTHIA calculations with different options. The solid curve is a NLO pQCD calculation.

We used the ratio $R = N(D^0)/N(c\bar{c}) = 0.54 \pm 0.05$ from e^+e^- collisions [15] to convert the D^0 yield to total $c\bar{c}$ yield. The d+Au number of binary collisions N_{bin} and the p+p inelastic scattering cross section was used to convert the $dN^{c\bar{c}}/dy$ in d+Au collisions in to $d\sigma^{c\bar{c}}/dy$ in p+p collisions. A factor of 4.7 ± 0.7 [18, 19] was used to convert the $d\sigma/dy$ at midrapidity to the total cross section. The total charm cross section per nucleon-

nucleon interaction for d+Au collisions at 200 GeV is $1.3 \pm 0.2 \pm 0.4$ mb from D^0 alone and $1.4 \pm 0.2 \pm 0.4$ mb from the combined fit of D^0 and electrons.

The beam energy dependence of the charm cross section from this analysis is depicted in Fig. 3 by the star symbol and compared to PHENIX [20], UA2 [21], FNAL and SPS [22] measurements. The dotted line is a power law fit, $\sigma_{cc}^{NN} \propto (\sqrt{s})^n$, to the data points with $n=1.9 \pm 0.2$, while $n \sim 0.3(0.5)$ had been observed for charged hadron (pion) productions [7]. This indicates a harder behavior of the underlying process going from charged hadron production to charm dominated processes. The dashed and dash-dotted curves depict PYTHIA calculations with and without higher order processes [19]. The solid curve depicts the next-to-leading order (NLO) pQCD calculation from Ref. [18]. At $\sqrt{s}=200$ GeV, both calculations underpredict the total charm cross section by at least a factor of 3.

3.2. Open Charm p_T Spectrum

The invariant yield distributions as a function of p_T for $D^{*\pm}$, D^\pm and the high p_T D^0 were obtained using the same methods as that for the low p_T D^0 . With all the data points from the direct open charm measurements shown in Fig. 4, the p_T distribution was fit to a power-law function, $A(1 + p_T/p_0)^{-n}$, with the ratio of $D^*/D^0 = D^+/D^0$ as a free parameter, where A , p_0 and n are fit parameters. From the fit, we obtained $dN/dy(D^0)=0.027 \pm 0.004 \pm 0.007$ which is consistent with the exponential fit results to the low p_T D^0 data points only, $\langle p_T \rangle = 1.32 \pm 0.08 \pm 0.16$ GeV/c, and the

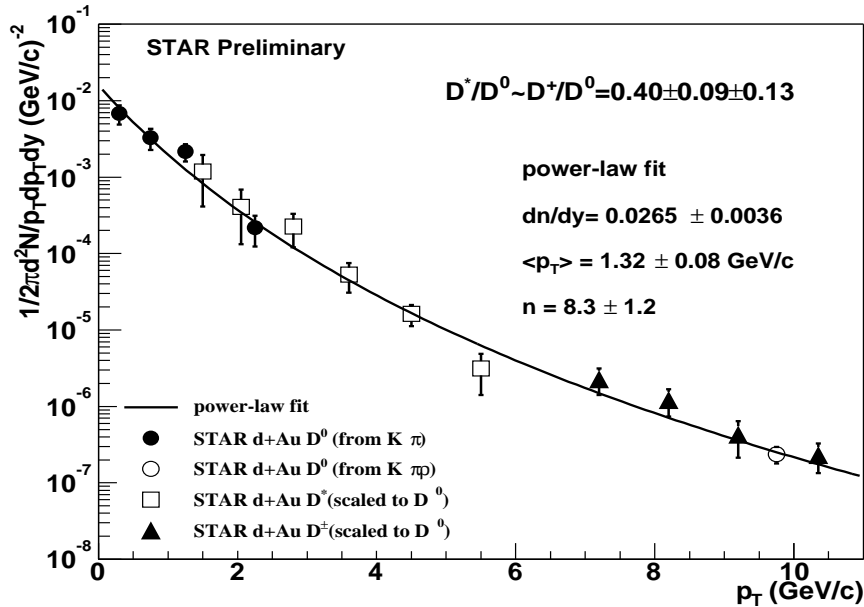


Figure 4. The measured invariant yield distributions for D^0 , $D^{*\pm}$ and D^\pm and a power-law fit to the data points. The D^* and D^\pm data points were scaled by the ratio $D^*/D^0 = D^\pm/D^0 = 0.40 \pm 0.09 \pm 0.13$ after the power-law fit.

ratio $D^*/D^0 = D^+/D^0 = 0.40 \pm 0.09 \pm 0.13$ which agrees with the ratios from previous measurements [23] and theoretical predictions [24] within the experimental uncertainties.

4. Conclusion

The direct open charm D^0 , $D^{*\pm}$ and D^\pm signals were reconstructed in d+Au collisions at $\sqrt{s_{NN}}=200$ GeV using the STAR TPC. Single electron/positron spectra were measured using the TOFr+TPC for $p_T < 3$ GeV/c and using the TPC only for $2 < p_T < 4$ GeV/c in d+Au and p+p collisions at the same beam energy. From the low p_T D^0 and the single electron measurements, a total $c\bar{c}$ cross section was obtained and is at least about a factor of 3 larger than PYTHIA and NLO pQCD calculations. The D^0 , $D^{*\pm}$ and D^\pm open charm p_T spectra in d+Au collisions was fit to a power-law fit and the $D^*/D^0 = D^+/D^0 = 0.40 \pm 0.09 \pm 0.13$ was extracted and agrees with the ratios from previous measurements and theoretical predictions within the experimental uncertainties.

- [1] Frixióne S *et al.* 1997 *Preprint* hep-ph/9702287
- [2] Vogt R 1996 *Z. Phys. C* **71** 475
- [3] Lin Z *et al.* 1995 *Phys. Rev. C* **51** 2177
- [4] Dokshizer Y L *et al.* 2001 *Phys. Lett. B* **519** 199
- [5] Braun-Munzinger P *et al.* 2000 *Phys. Lett. B* **490** 196.
- [6] Braun-Munzinger P *et al.* 2001 *Nucl. Phys. A* **690** 119c.
- [7] Andronic A *et al.* 2003 *Phys. Lett. B* **571** 36
- [8] Thews R L *et al.* 2001 *Phys. Rev. C* **63** 054905
- [9] Gorenstein M I *et al.* 2002 *J Phys. G* **28** 2151
- [10] Matsui T *et al.* 1986 *Phys. Lett. B* **178** 416
- [11] Adams J *et al.* (STAR Collaboration) 2003 submitted to *Phys. Rev. Lett.* nucl-ex/0309012
- [12] Adler C *et al.* (STAR Collaboration) 2002 *Phys. Rev. C* **66** 061901 (R)
- [13] Zhang H 2004 *J. Phys. G* **30** S577
- [14] Zhang H 2003 Ph.D. thesis, Yale University
- [15] Hagiwara K *et al.* (Particle Data Group) 2002 *Phys. Rev. D* **66** 010001
- [16] Bonner B *et al.* 2003 *Nucl. Instr. Meth. A* **508** 181
- [17] Shao M *et al.* 2002 *Nucl. Instr. Meth. A* **492** 344
- [18] Vogt R 2002 *Preprint* hep-ph/0203151
- [19] Sjöstrand T *et al.* 2001 *Comp. Phys. Comm.* **135** 238
- [20] Adcox K *et al.* (PHENIX Collaboration) 2002 *Phys. Rev. Lett.* **88** 192303
- [21] Botner O *et al.* 1990 *Phys. Lett. B* **236** 488
- [22] Alves G A *et al.* (E769 Collaboration) 1996 *Phys. Rev. Lett.* **77** 2388
- [23] Acosta D *et al.* (CDF Collaboration) 2003 *Phys. Rev. Lett.* **91** 241894
- [24] Andronic A *et al.* 2003 *Nucl. Phys. A* **715** 529